

Supporting Information

Harnessing the Reversible Isomerization of Spiropyran to Merocyanine in Conjugated Polymers for Broadband Ultra-Violet to Near-Infrared Electrochromic Switching

Raul S. Ramos,^a Fernando Muñoz-Alba,^b Kavish Saini,^a Karyme M. Castaneda,^a Vianey F. Juarez-Rangel,^a Sreeprasad T. Sreenivasan,^a M. Carmen Ruiz Delgado,^{bc} Rocío Ponce Ortiz,^{bc}
and Robert M. Pankow^{a*}

^aDepartment of Chemistry and Biochemistry, University of Texas at El Paso, El Paso, Texas
79968, USA.

^bDepartment of Physical Chemistry, Faculty of Sciences, University of Málaga, 29071 Málaga,
Spain

^cInstituto Universitario de Materiales y Nanotecnología, IMANA, University of Málaga, Campus
de Teatinos, 29071, Málaga, Spain.

*To whom correspondence may be addressed:

R. M. P. (rmpankow@utep.edu)

Table of Contents

| | |
|---|-----------|
| 1. General..... | 3 |
| 2. DFT Calculations | 4 |
| 3. Monomer Synthesis..... | 7 |
| 4. Monomer NMR Spectra..... | 11 |
| 5. Cyclic Voltammetry | 17 |
| 6. Electrochromic Characterization | 19 |
| 7. Atomic Force Microscopy | 21 |
| 8. References | 22 |

1. General

All solvents, reagents and chemicals were purchased from commercial sources (Fisher Scientific, VWR, Sigma-Aldrich, and Ambeed) and used as received. Anhydrous acetonitrile (MeCN) and propylene carbonate (PC) were purchased from Thermo Fisher Scientific and used as received. 5-Bromo-2,3,3-trimethyl-3*H*-indole (**S1**), 5-bromosalicylaldehyde (**S3**), 3-bromo-2-hydroxybenzaldehyde (**S4**), 2,2'-bithiophene-5-boronic acid pinacol ester, and 2-thiophene-5-boronic acid pinacol ester were purchased from Ambeed and used as received. Unless specified otherwise, all reactions were performed using oven dried glassware under a N₂ atmosphere. Anhydrous piperidine, dichloromethane (DCM) and ethanol (EtOH) were obtained by storing over 3 Å molecular sieves under a nitrogen atmosphere for a minimum 24 hours. All NMR spectra were recorded at 25 °C using CDCl₃ on a Bruker Avance III 400 MHz. All spectra were referenced to CHCl₃ (7.26 ppm). ESI-HRMS was performed on a JEOL AccuTOF TC-100 using HPLC grade MeOH (SP2T and SPr2T) or HPLC grade THF (SP4T and SPr4T) and calibrated to PEG 400.

2. DFT Calculations

Calculations were carried out in the frame of density functional theory (DFT) using the long-range corrected hybrid ω B97X-D⁵ functional together with 6-31G** basis set^{6,7} as implemented in the Gaussian 16 suite of programs.⁸ Geometry optimizations were performed along with a conformational search to the thiophene-spacer bond torsions without any symmetry constraints with the aim to find the absolute minimum. The ethyl alkyl chains on the indole N-atom were replaced with methyl groups to simplify the calculations. Harmonic vibrational frequencies were calculated at the same theoretical level based on the ground-state geometries of the most stable conformers corroborating that the optimized geometries are absolute minima (zero imaginary frequencies). The vertical transition energies and oscillator strengths between the initial and excited states were computed by using the time-dependent DFT approach (TD-DFT).^{9–11} Molecular orbitals distributions were visualized using ChemCraft 1.8 molecular modelling software.¹²

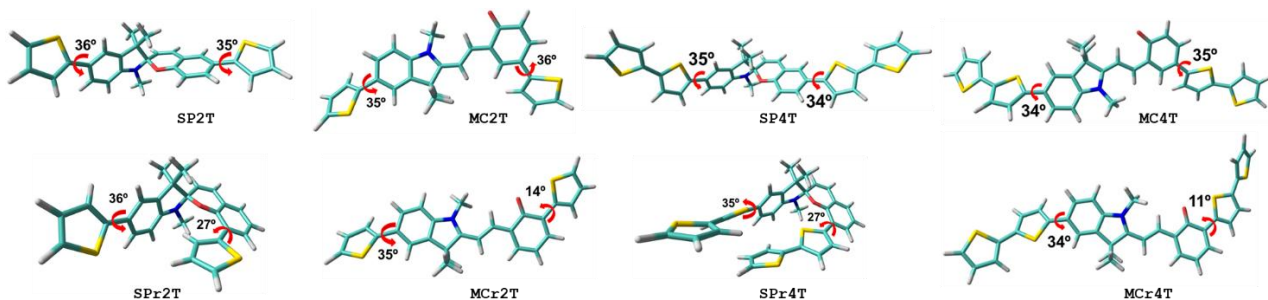


Figure S1. DFT-calculated torsion angles for model compounds SP2T, MC2T, SP4T, MC4T, SPr2T, MCr2T, MCr4T, and SPr4T.

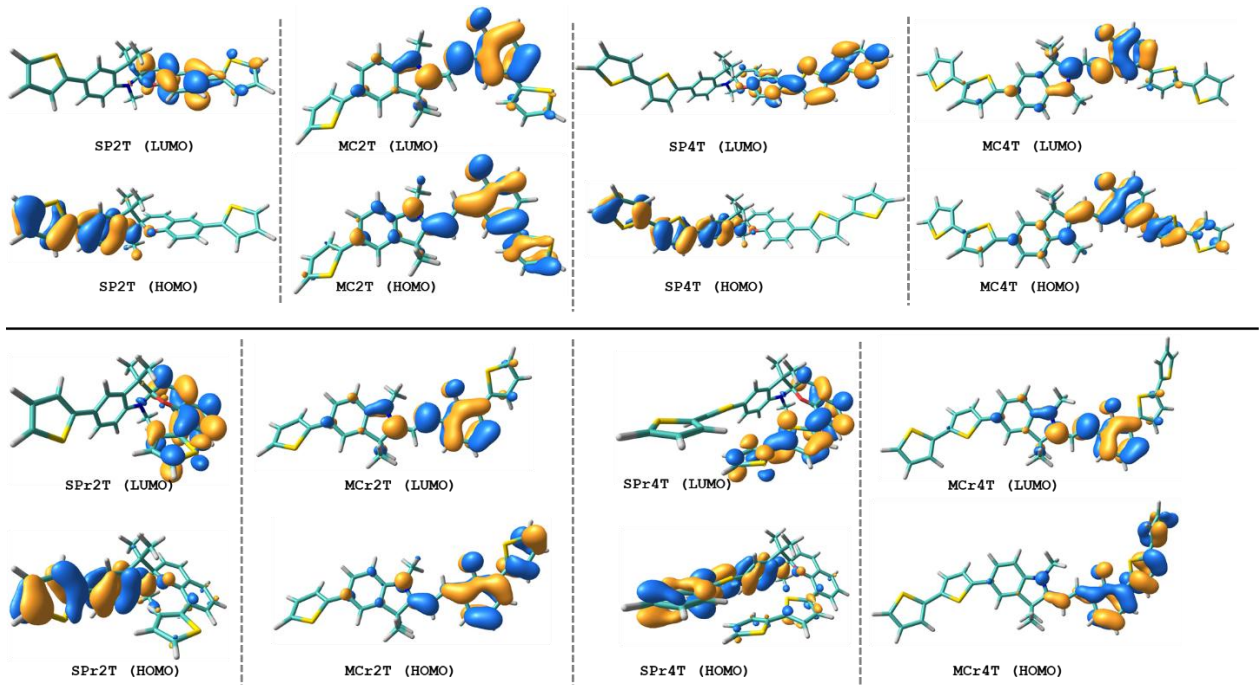


Figure S2. DFT-calculated frontier molecular orbital topologies for model compounds SP2T, MC2T, SP4T, MC4T, SPr2T, MCr2T, SPr4T, and MCr4T.

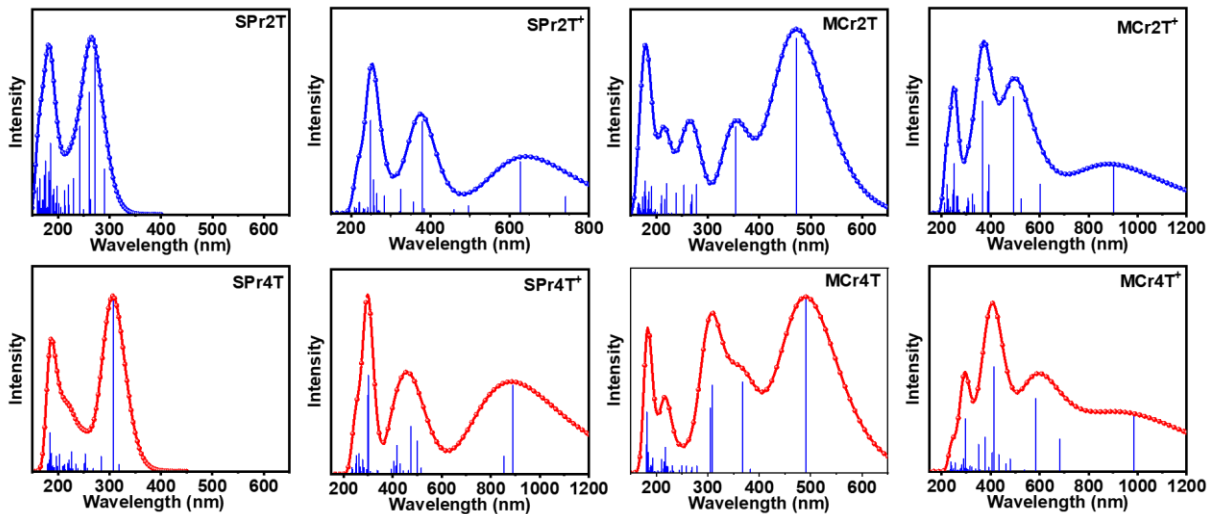


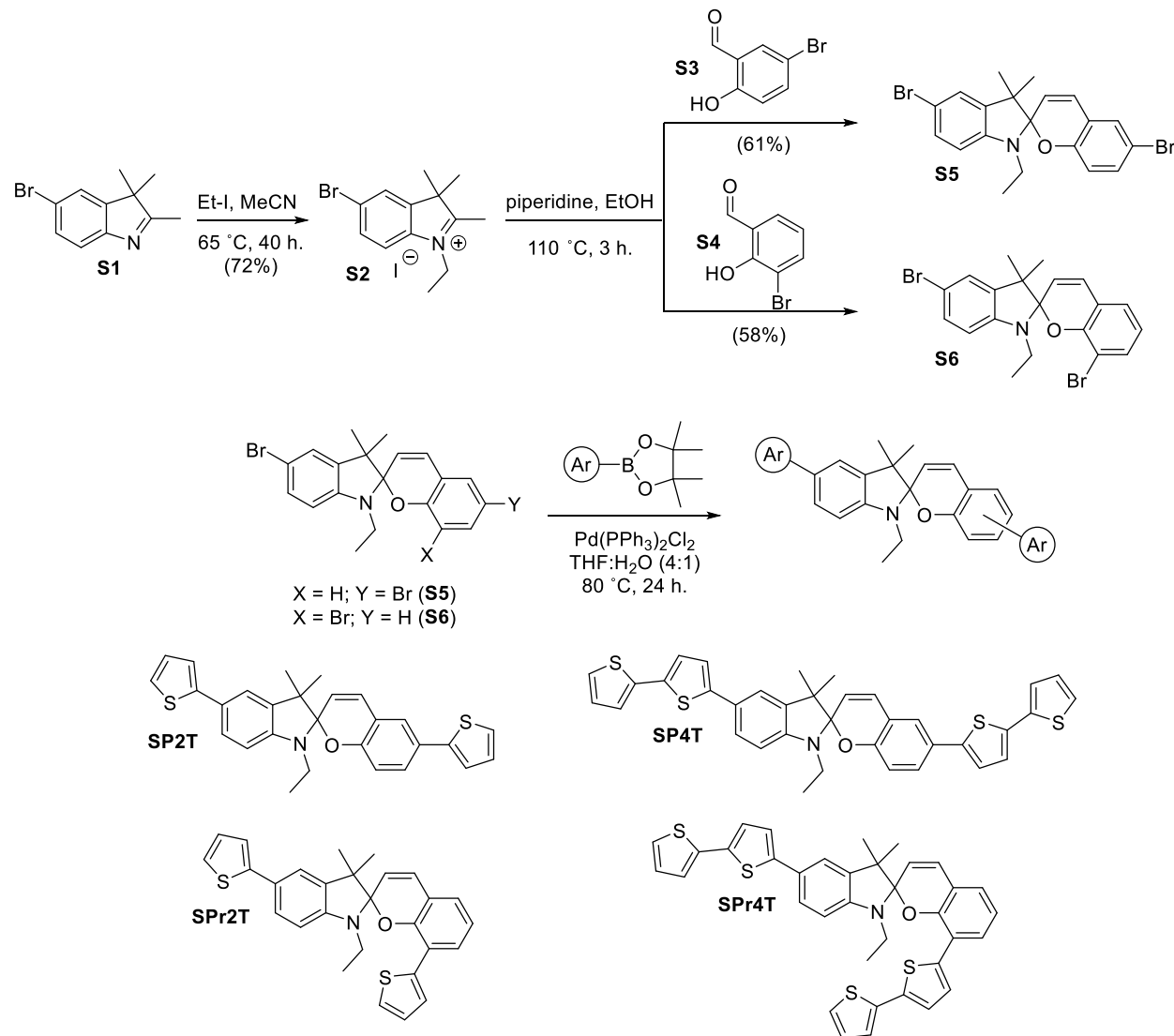
Figure S3. TD-DFT simulated optical absorption spectra and main excitations (wavelength vs. oscillator strength) shown as vertical bars for model compounds SPr2T, SPr2T⁺, MCr2T, MCr2T⁺, SPr4T, SPr4T⁺, MCr4T, and MCr4T⁺.

Table S1. Maximum optical absorption wavelengths (λ_{\max}), frontier molecular orbital energies, and torsion angles for SP2T/SP2T⁺, MC2T/MC2T⁺, SP4T/SP4T⁺, MC4T/MC4T⁺, SPr2T/SPr2T⁺, MCr2T/MCr2T⁺, SPr4T/SPr4T⁺, and MCr4T/MCr4T⁺ calculated at the ω B97X-D/6-31G** level of theory.

| Entry | λ_{\max} (nm) | HOMO (eV) ^a | LUMO (eV) | Torsion Angles (°) |
|--------------------|-----------------------|------------------------|-----------|--------------------|
| SP2T | 191, 265 | -6.97 | 0.72 | 36, 35 |
| SP2T ⁺ | 272, 374, 626 | -9.58 | -2.82 | -1, 34 |
| MC2T | 178, 261, 455 | -6.54 | -0.67 | 35, 36 |
| MC2T ⁺ | 254, 334, 531 | -9.90 | -3.40 | 30, 6 |
| SP4T | 199, 310 | -6.82 | 0.38 | 35, 34 |
| SP4T ⁺ | 307, 463, 839 | -8.45 | -3.52 | 34, 1 |
| MC4T | 184, 316, 471 | -6.43 | -0.77 | 34, 35 |
| MC4T ⁺ | 295, 378, 532 | -9.11 | -3.69 | 29, 1 |
| SPr2T | 182, 265 | -7.05 | 0.63 | 36, 27 |
| SPr2T ⁺ | 253, 374, 640 | -10.09 | -2.85 | -3, 36 |
| MCr2T | 179, 471 | -6.54 | -0.73 | 35, 14 |
| MCr2T ⁺ | 249, 373, 498 | -9.95 | -3.98 | 30, 0 |
| SPr4T | 186, 307 | -6.82 | 0.44 | 35, 27 |
| SPr4T ⁺ | 297, 457, 885 | -9.50 | -3.00 | 18, 38 |
| MCr4T | 183, 307, 490 | -6.43 | 0.84 | 34, 11 |
| MCr4T ⁺ | 295, 407, 598, 979 | -9.06 | -3.79 | 30, 0 |

^a SOMO energies for the charged species (SP2T⁺, SPr2T⁺, SP4T⁺, SPr4T⁺, MC2T⁺, MCr2T⁺, MC4T⁺, and MCr4T⁺).

3. Monomer Synthesis



Scheme S1. Synthesis of spiropyran monomers SP2T, SP4T, SPr2T, and SPr4T.

5-Bromo-1-ethyl-2,3,3-trimethyl-3H-indolium Iodide (S2). To an oven dried single-neck 25 mL round bottom flask equipped with a stir-bar was added **S1** (1.2 g, 5.04 mmol), ethyl iodide (2 mL), and acetonitrile (2.5 mL). The flask was equipped with a condenser and the reaction mixture was heated at 65 °C for 40 h. The reaction mixture was then cooled to room temperature and the volatiles were removed via rotovap. The residue was triturated with diethyl ether to yield a gray solid that was used without further purification. 72% yield. Consistent with literature reports.¹

5',6-dibromo-1'-ethyl-1',3'-dihydro-3',3'-dimethyl-spiro[2H-1-benzopyran-2,2'-[2H]indole] (S5). **S2** (788 mg, 2 mmol, 1 equiv.) and **S3** (402 mg, 2 mmol, 1 equiv.) were added to an oven dried 50

mL round-bottom flask equipped with a stir-bar and condenser. The reaction apparatus was vacuum-backfilled 3x with nitrogen, and anhydrous piperidine (187 mg, 2.2 mmol, 2.2 equiv) and EtOH (20 mL) were added via syringe through a rubber septum. The reaction mixture was then degassed with nitrogen for 10 min. Then the reaction mixture was heated at 110 °C for 3 h. The volatiles were then removed via rotovap, and the solid residue was then recrystallized 2x from EtOH (20 mL) to afford **S2** in 61% yield. ¹H-NMR (CDCl₃, 25 °C, 400 MHz): δ (ppm) 7.24 (dd, *J* = 8.0, 2.0 Hz, 1H), 7.19-7.16 (m, 2H), 7.12 (d, *J* = 4.0 Hz), 6.76 (d, *J* = 12.0 Hz, 1H), 6.56 (d, *J* = 12 Hz, 1H), 6.40 (d, *J* = 8.0 Hz, 1H), 5.68 (d, *J* = 12 Hz, 1H), 3.33-3.24 (m, 1H), 3.18-3.09 (m, 1H), 1.25 (s, 3H), 1.15-1.11 (m, 6H). ¹³C-NMR (CDCl₃, 25 °C, 100 MHz): δ (ppm) 153.0, 146.0, 138.8, 132.3, 130.1, 129.1, 128.5, 124.9, 120.5, 120.2, 116.9, 111.9, 110.3, 107.7, 104.8, 52.3, 37.8, 25.8, 19.8, 14.1. The NMR is consistent with previous reports.²

*5',8-dibromo-1'-ethyl-1',3'-dihydro-3',3'-dimethyl-spiro[2H-1-benzopyran-2,2'-[2H]indole] (**S6**).* Identical to the synthesis of **S5** but with **S4** in place of **S3**. 58% yield. ¹H-NMR (CDCl₃, 25 °C, 400 MHz): δ (ppm) 7.32 (dd; *J* = 8.0 Hz, 1.6 Hz, 1H), 7.23 (dd, *J* = 8.0, 2.4 Hz, 1H), 7.13 (d, *J* = 2.0 Hz, 1H), 6.98 (dd, *J* = 8.0, 2.0 Hz, 1H), 6.79 (d, *J* = 12.0 Hz, 1H), 6.71 (dd, *J* = 8.4, 7.6 Hz, 1H), 6.41 (d, *J* = 8.0 Hz, 1H), 5.66 (d, *J* = 8.0 Hz, 1H), 3.35-3.26 (m, 1H), 3.22-3.13 (m, 1H), 1.28 (s, 3H), 1.15-1.12 (m, 6H). ¹³C-NMR (CDCl₃, 25 °C, 100 MHz): δ (ppm) 150.3, 145.9, 133.8, 133.1, 130.0, 129.0, 125.8, 124.9, 120.9, 120.3, 119.9, 110.2, 109.4, 107.7, 105.6, 52.3, 37.7, 25.8, 20.0, 13.7. The NMR is consistent with previous reports.²

*5',6-bis(2-thienyl)-1'-ethyl-1',3'-dihydro-3',3'-dimethyl-spiro[2H-1-benzopyran-2,2'-[2H]indole] (**SP2T**).* Adapted from literature procedures.³ A 2-neck round-bottom flask equipped with a stir-bar and condenser was charged with **S5** (487 mg, 1.11 mmol, 1 equiv.), 2-thiophene-5-boronic acid pinacol ester (713 mg, 5.57 mmol, 5 equiv.), and Pd(PPh₃)₂Cl₂ (77 mg, 0.11 mmol, 0.10 equiv.). The flask was vacuum-backfilled with nitrogen 3x and a previously degassed (4:1) mixture of THF:H₂O (6.5 mL) was then added. The reaction mixture was then heated at 80 °C for 24 h. After cooling to room temperature, the reaction mixture was precipitated in MeOH (20 mL) and stirred for 30 min. The tan precipitate was then filtered off, washed with MeOH (5x10 mL), and dried under vacuum. Yield: 57%. ¹H-NMR (CDCl₃, 25 °C, 400 MHz): δ (ppm) 7.43 (dd, *J* = 8.0, 1.6 Hz, 1H), 7.36 (dd, *J* = 8.0, 1.6 Hz, 1H), 7.30-7.29 (m, 2H), 7.22-7.17 (m, 4H), 7.06-7.03 (m, 2H), 6.89 (d, *J* = 10.4 Hz, 1H), 6.72 (d, *J* = 8.0 Hz, 1H), 6.55 (d, *J* = 8.0 Hz, 1H), 5.74 (d, *J* = 10.0 Hz, 1H),

3.42-3.33 (m, 1H), 3.27-3.18 (m, 1H), 1.36, (s, 3H), 1.21-1.17 (m, 6H). ^{13}C -NMR (CDCl_3 , 25 °C, 100 MHz): δ (ppm) 153.75, 146.8, 145.8, 144.2, 137.3, 129.2, 127.9, 127.8, 127.5, 126.8, 125.8, 125.5, 124.9, 123.7, 122.8, 121.9, 121.1, 120.2, 119.9, 118.7, 115.5, 106.3, 104.8, 52.2, 37.9, 26.1, 20.0, 14.3. ESI-HRMS (m/z) for $\text{C}_{28}\text{H}_{25}\text{NOS}_2$ calculated: 455.14; found (M+H $^+$): 456.134.

5',8- bis(2-thienyl)-1'-ethyl-1',3'-dihydro-3',3'-dimethyl-spiro[2H-1-benzopyran-2,2'-[2H]indole] (SPr2T). Identical procedure to **SP2T** but with **S6** in place of **S5**. Yield: 72%. ^1H -NMR (CDCl_3 , 25 °C, 400 MHz): δ (ppm) 7.59 (dd, J = 8.0, 1.2 Hz, 1H), 7.46 (dd, J = 8.0, 1.9 Hz, 1H), 7.33 (d, J = 1.8 Hz, 1H), 7.29 (dd, J = 3.8, 1.1 Hz, 1H), 7.21 (dd, J = 3.6, 1.2 Hz, 1H), 7.18 (dd, J = 5.1, 1.1 Hz, 1H), 7.07-7.04 (m, 2H), 6.99 (dd, J = 7.4, 1.6 Hz, 1H), 6.92-6.84 (m, 3H), 6.57 (d, J = 8.0 Hz, 1H), 5.80 (d, J = 10.3 Hz, 1H), 3.40-3.31 (m, 1H), 3.25-3.16 (m, 1H), 1.34 (s, 3H), 1.25 (s, 3H), 1.17 (t, J = 7.2 Hz, 3H). ^{13}C -NMR (CDCl_3 , 25 °C, 100 MHz): δ (ppm) 149.4, 147.2, 146.0, 138.5, 137.5, 129.9, 127.8, 127.5, 126.4, 125.61, 125.59, 125.51, 125.48, 124.33, 122.7, 121.0, 120.9, 120.1, 119.9, 119.3, 119.2, 106.6, 106.0, 52.0, 38.0, 25.8, 19.8, 14.3. ESI-HRMS (m/z) for $\text{C}_{28}\text{H}_{25}\text{NOS}_2$ calculated: 455.14; found (M+H $^+$): 456.134.

5',6-bis(2,2'-bithiophene)-1'-ethyl-1',3'-dihydro-3',3'-dimethyl-spiro[2H-1-benzopyran-2,2'-[2H]indole] (SP4T). Identical procedure to **SP2T** but with 2,2'-bithiophene-5-boronic acid pinacol ester in place of 2-thiophene-5-boronic acid pinacol ester. Yield: 18%. ^1H -NMR (CDCl_3 , 25 °C, 400 MHz): δ (ppm) 7.42, (dd, J = 8.1 Hz, 1.9 Hz, 1H), 7.35 (dd, J = 8.4, 2.3 Hz, 1H), 7.29 (dd, J = 4.8, 1.8 Hz, 2H), 7.22-7.17 (m, 4H), 7.13-7.08 (m, 4H), 7.04-7.01 (m, 2H), 6.89 (d, J = 10.2 Hz, 1H), 6.73 (d, J = 8.4 Hz, 1H), 6.55 (d, J = 8.1 Hz, 1H), 5.74 (d, J = 10.3 Hz, 1H), 3.43-3.33 (m, 1H), 3.28-3.19 (m, 1H), 1.37 (s, 3H), 1.21-1.81 (m, 6H). ^{13}C -NMR (CDCl_3 , 25 °C, 100 MHz): δ (ppm) 153.8, 147.0, 144.7, 143.0, 137.9, 137.6, 137.3, 135.6, 134.6, 129.1, 127.81, 127.76, 127.2, 126.4, 125.6, 125.1, 124.53, 124.50, 124.1, 124.0, 123.8, 123.3, 123.0, 122.5, 121.6, 120.2, 119.6, 118.8, 115.6, 106.4, 104.8., 52.2, 37.9, 26.1, 20.0, 14.3. ESI-HRMS (m/z) for $\text{C}_{28}\text{H}_{25}\text{NOS}_2$ calculated: 619.11; found (M+H $^+$): 620.110.

5',8-bis(2,2'-bithiophene)-1'-ethyl-1',3'-dihydro-3',3'-dimethyl-spiro[2H-1-benzopyran-2,2'-[2H]indole] (SPr4T). Identical procedure to **SP2T** but with **S6** in place of **S5** and 2,2'-bithiophene-5-boronic acid pinacol ester in place of 2-thiophene-5-boronic acid pinacol ester. Yield: 18% ^1H -NMR (CDCl_3 , 25 °C, 400 MHz): δ (ppm) 7.62 (dd, J = 8.0, 1.6 Hz, 1H), 7.51 (dd, J = 8.0, 1.6 Hz, 1H), 7.44 (d, J = 1.8 Hz, 1H), 7.28 (d, J = 4.0 Hz, 1H), 7.22-7.19 (m, 2H), 7.17-

7.15 (m, 2H), 7.04 (dd, $J = 5.2$, 3.7 Hz, 1H), 7.00 (dd, $J = 7.4$, 1.5 Hz, 1H), 6.98-6.93 (m, 3H), 6.89 (dd, $J = 7.9$, 7.4 Hz, 1H), 6.66 (dd, $J = 4.0$, 1.2 Hz, 1H), 6.62-6.57 (m, 2H), 5.85 (d, $J = 10.2$ Hz, 1H), 3.36-3.27 (m, 1H), 3.23-3.14 (m, 1H), 1.41 (s, 3H), 1.28 (s, 3H), 1.14 (t, $J = 7.2$ Hz, 3H). ^{13}C -NMR (CDCl_3 , 25 °C, 100 MHz): δ (ppm) 148.9, 147.5, 144.8, 138.0, 137.9, 137.8, 137.5, 136.5, 134.4, 130.2, 127.81, 127.77, 126.2, 125.5, 125.4, 125.3, 124.5, 124.2, 123.74, 123.72, 123.5, 123.2, 123.0, 122.2, 121.5, 120.5, 120.1, 119.1, 118.6, 107.1, 106.2, 51.8, 38.0, 25.8, 19.5, 14.3. ESI-HRMS (m/z) for $\text{C}_{28}\text{H}_{25}\text{NOS}_2$ calculated: 619.11; found ($\text{M}+\text{H}^+$): 620.110.

4. Monomer NMR Spectra

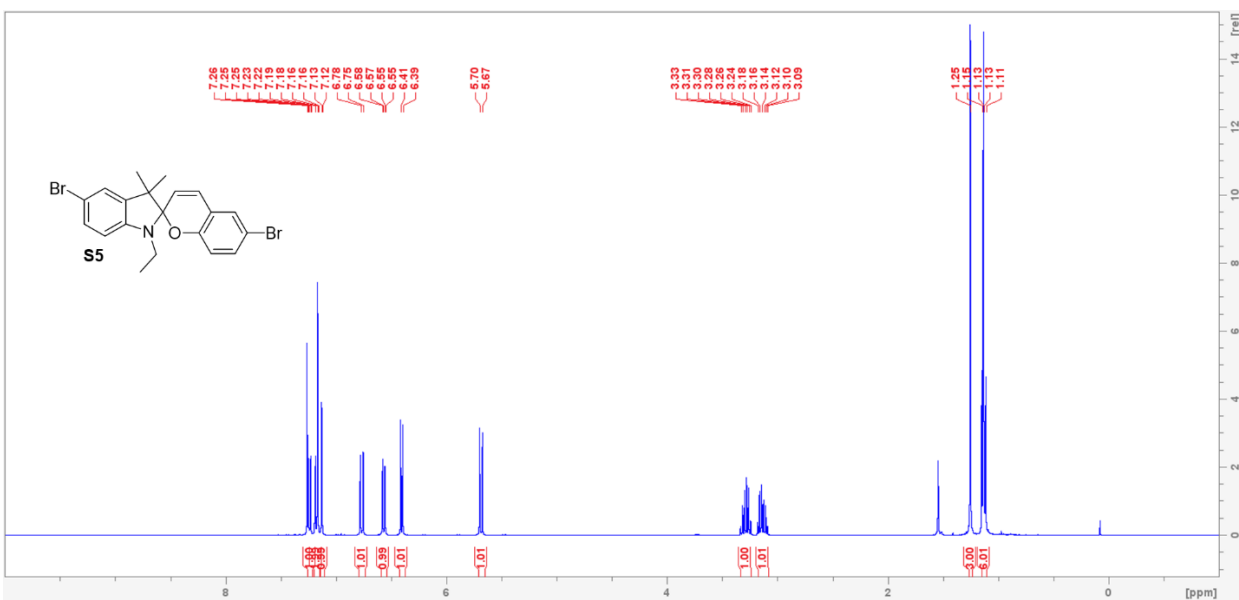


Figure S4. ^1H -NMR of S5 in CDCl_3 at 400 MHz and 25 °C.

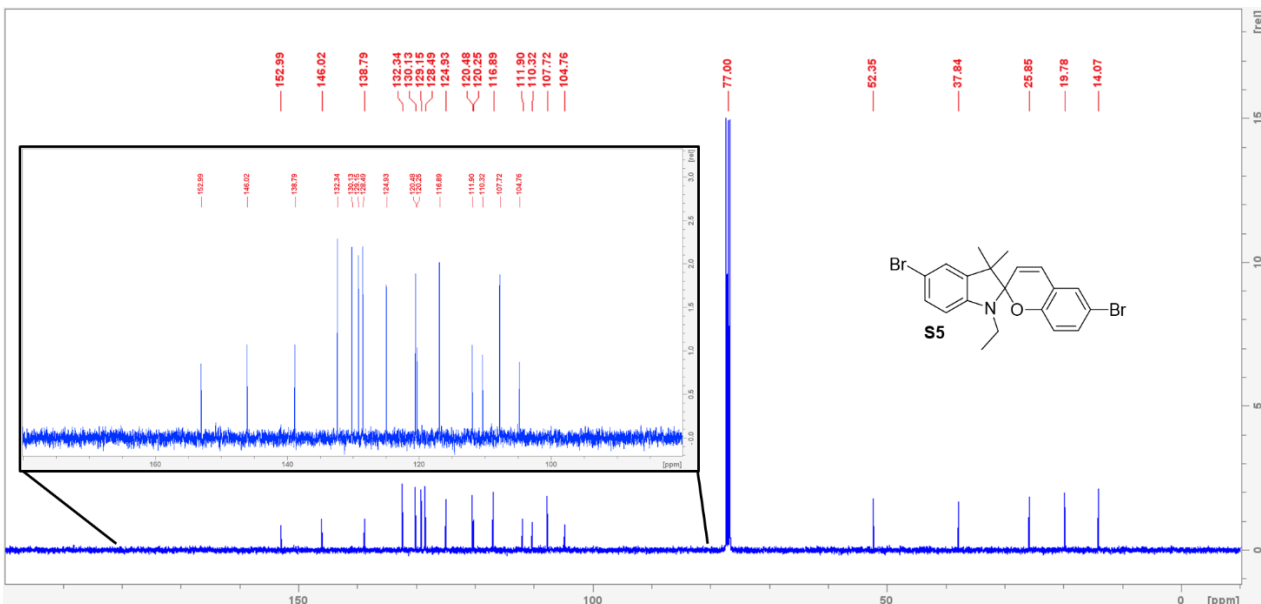


Figure S5. ^{13}C -NMR of S5 in CDCl_3 at 100 MHz and 25 °C.

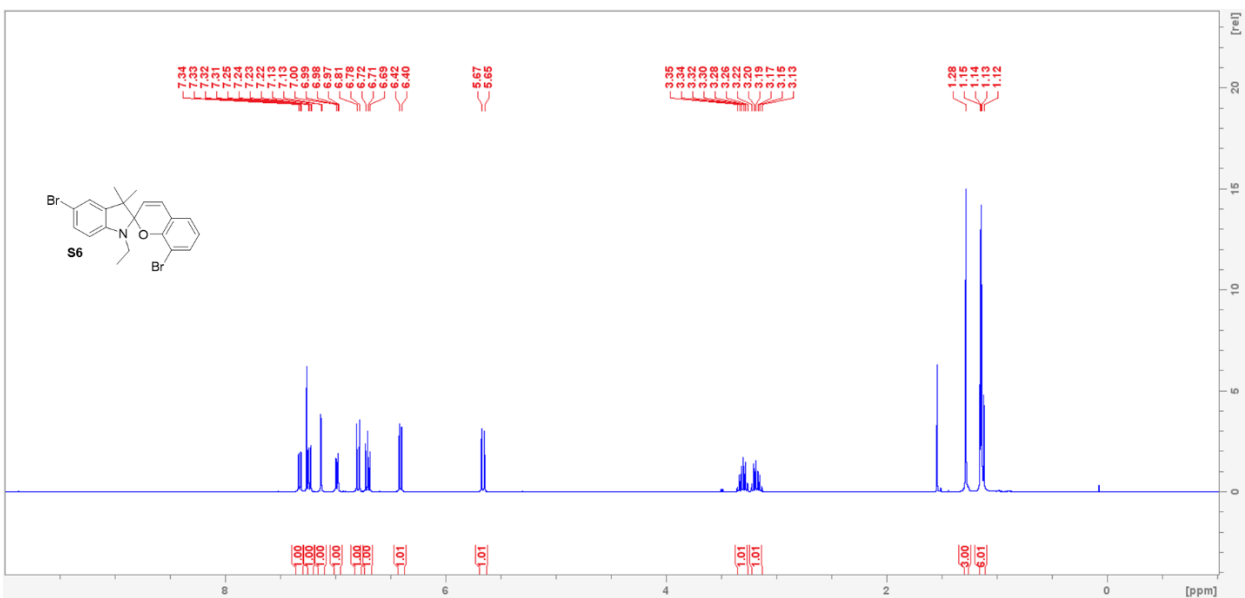


Figure S6. ^1H -NMR of S6 in CDCl_3 at 400 MHz and 25 °C.

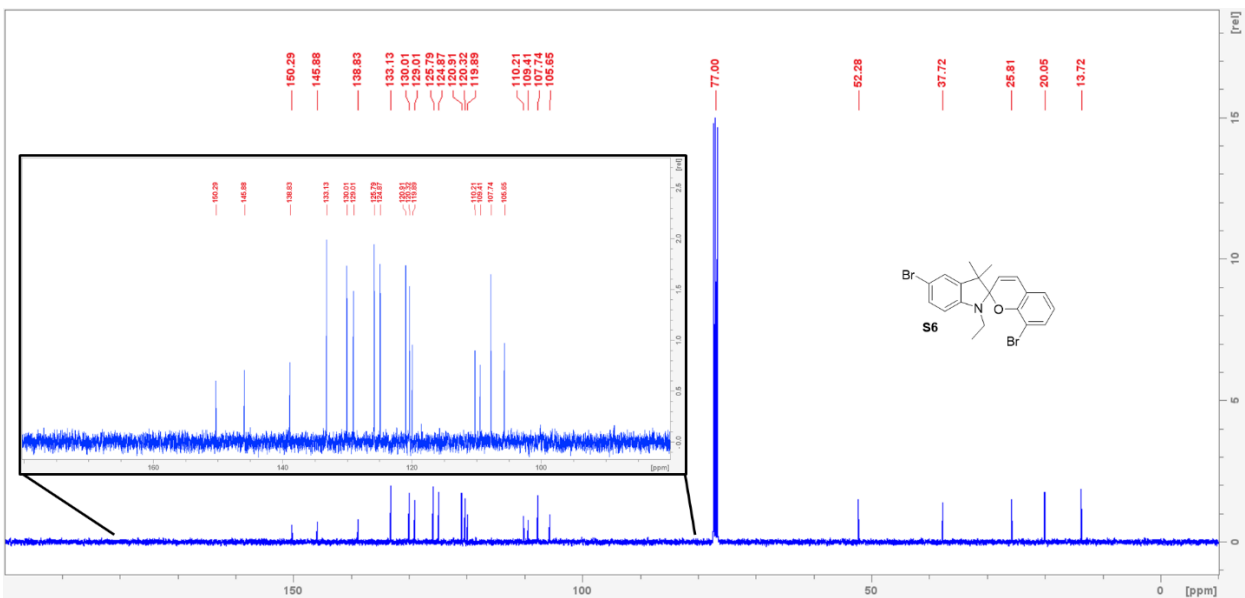


Figure S7. ^{13}C -NMR of S6 in CDCl_3 at 100 MHz and 25 °C.

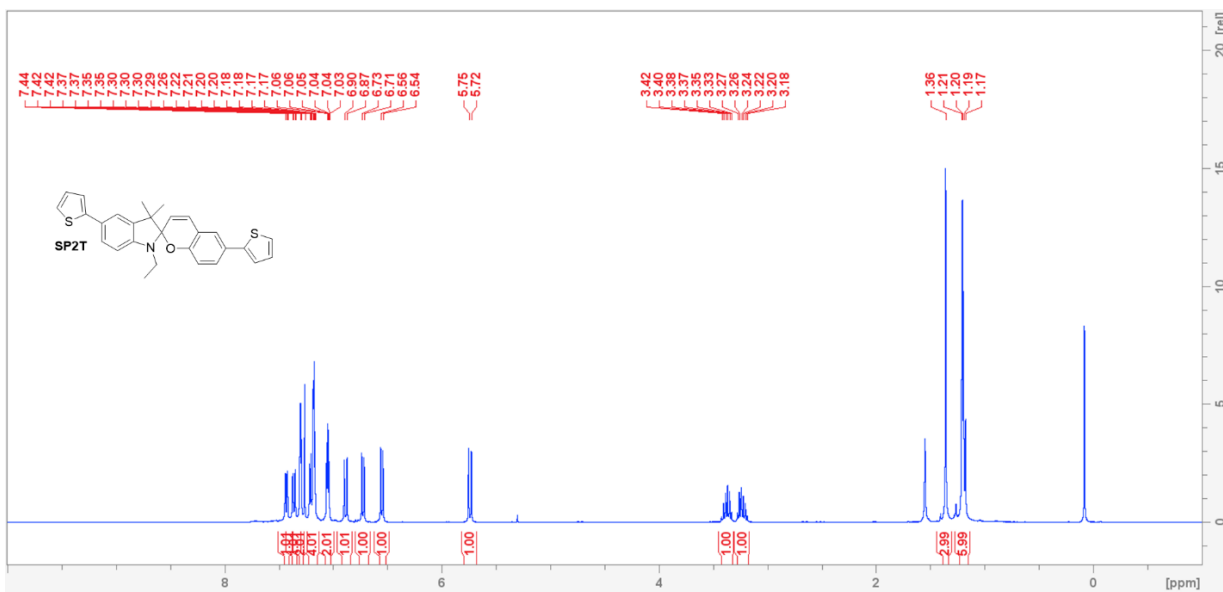


Figure S8. ^1H -NMR of SP2T in CDCl_3 at 400 MHz and 25 °C.

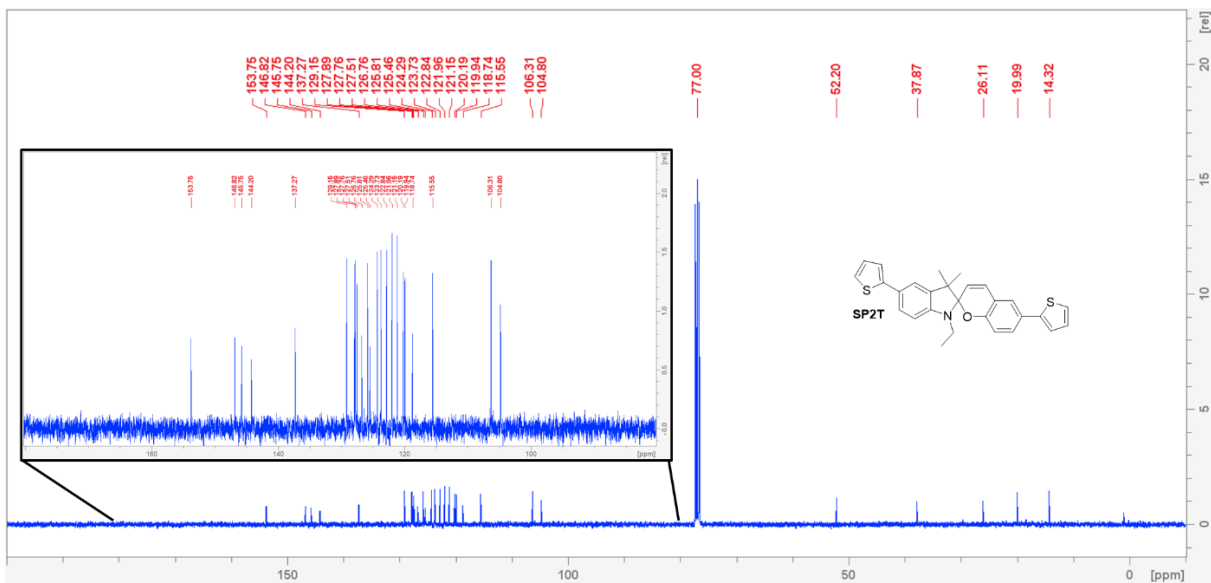


Figure S9. ^{13}C -NMR of SP2T in CDCl_3 at 100 MHz and 25 °C.

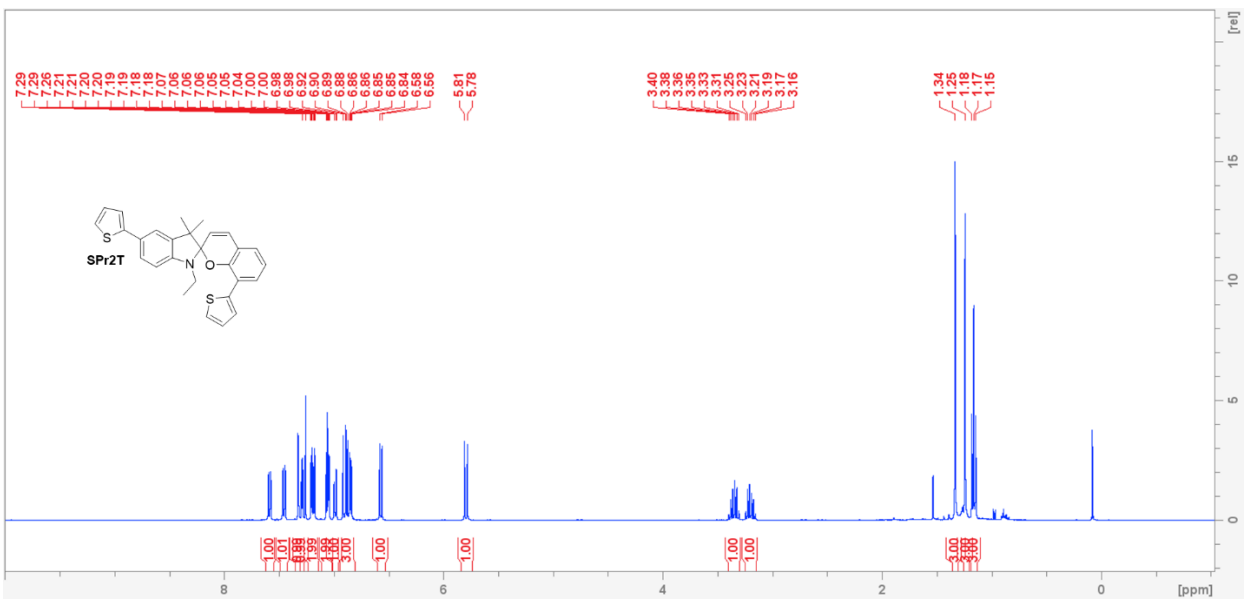


Figure S10. ^1H -NMR of SPr2T in CDCl_3 at 400 MHz and 25 °C.

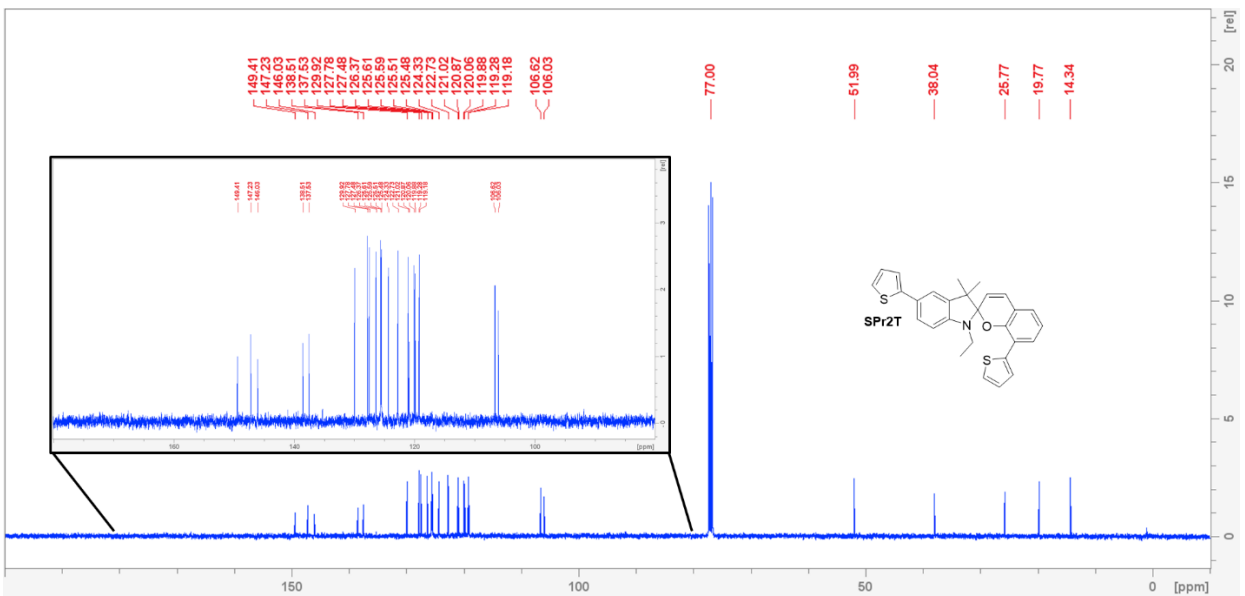


Figure S11. ^{13}C -NMR of SPr2T in CDCl_3 at 100 MHz and 25 °C.

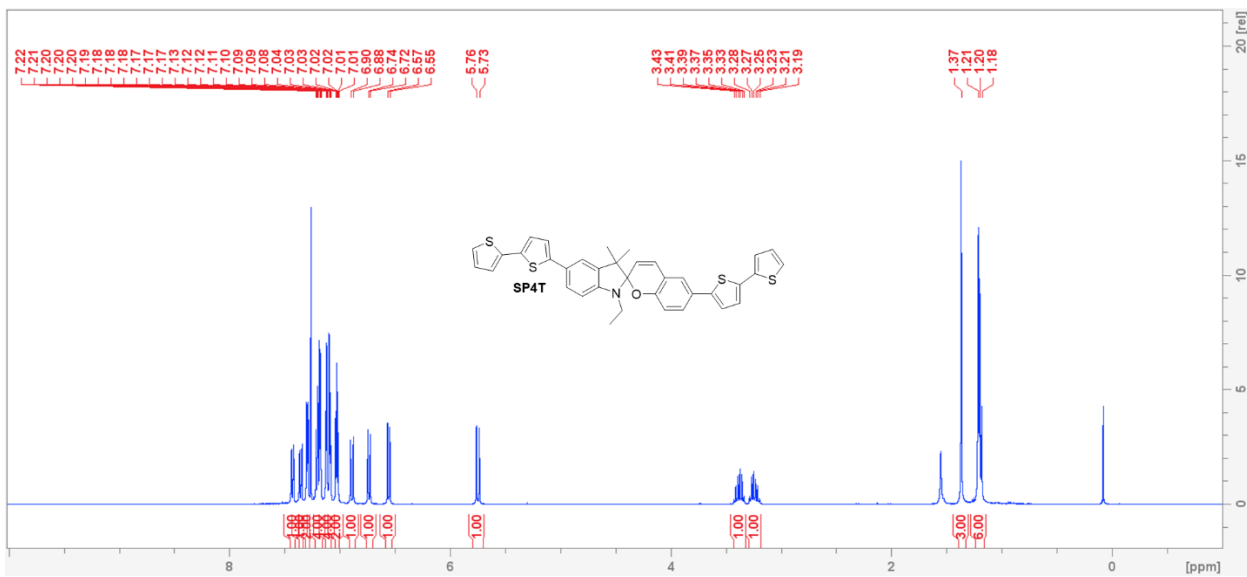


Figure S12. ^1H -NMR of SP4T in CDCl_3 at 400 MHz and 25 °C.

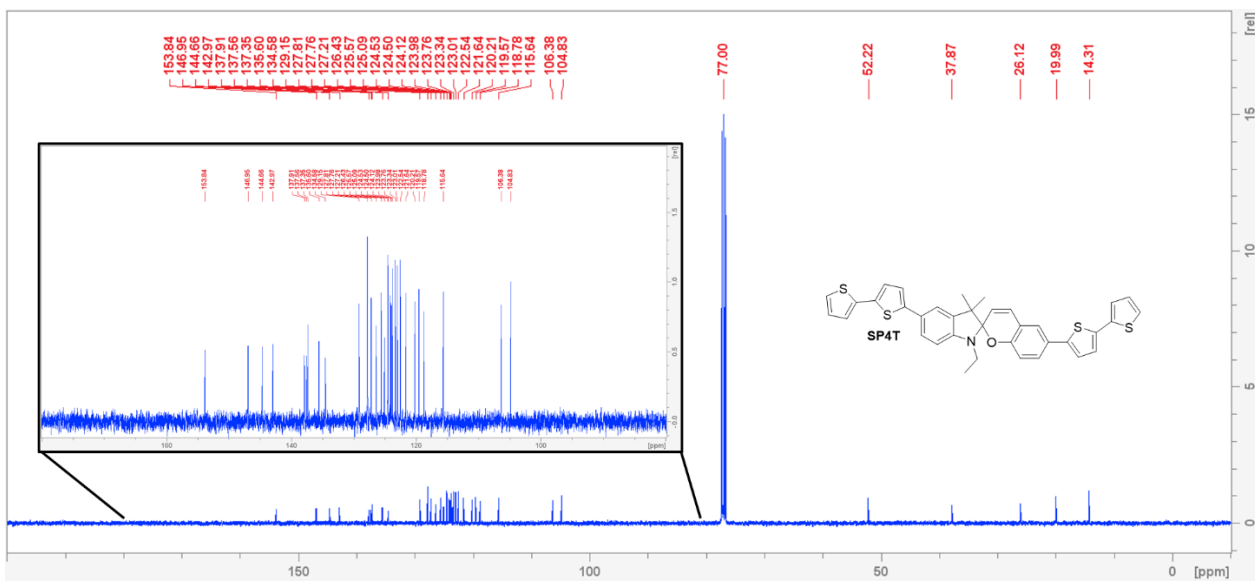


Figure S13. ^{13}C -NMR of SP4T in CDCl_3 at 100 MHz and 25 °C.

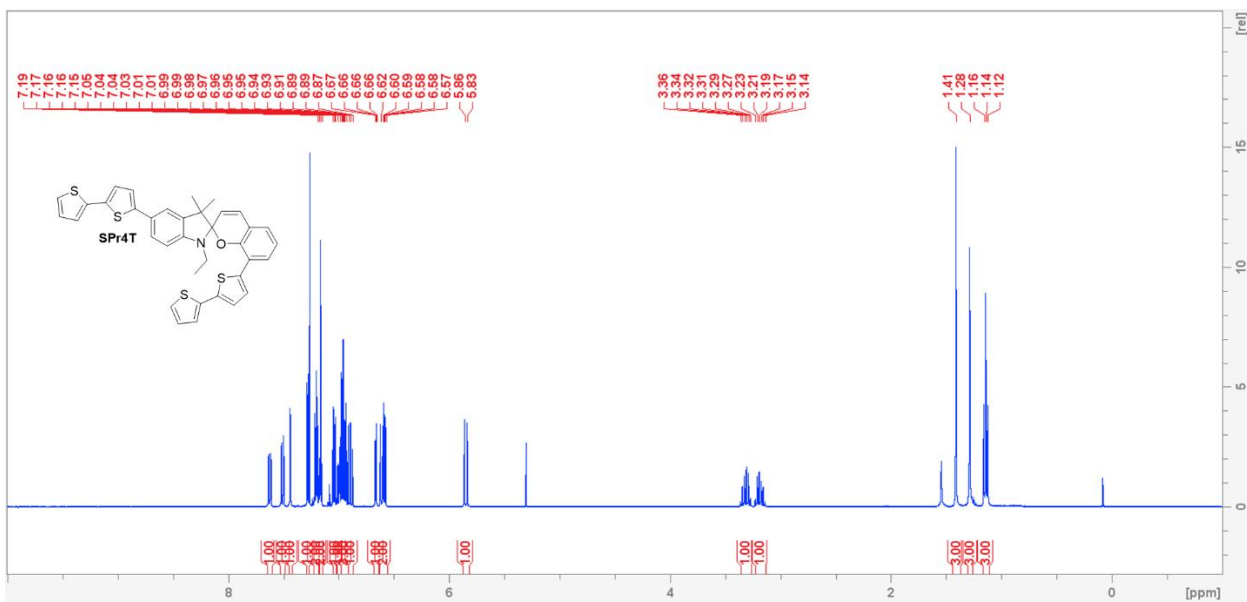


Figure S14. ^1H -NMR of SPr4T in CDCl_3 at 400 MHz and 25 °C.

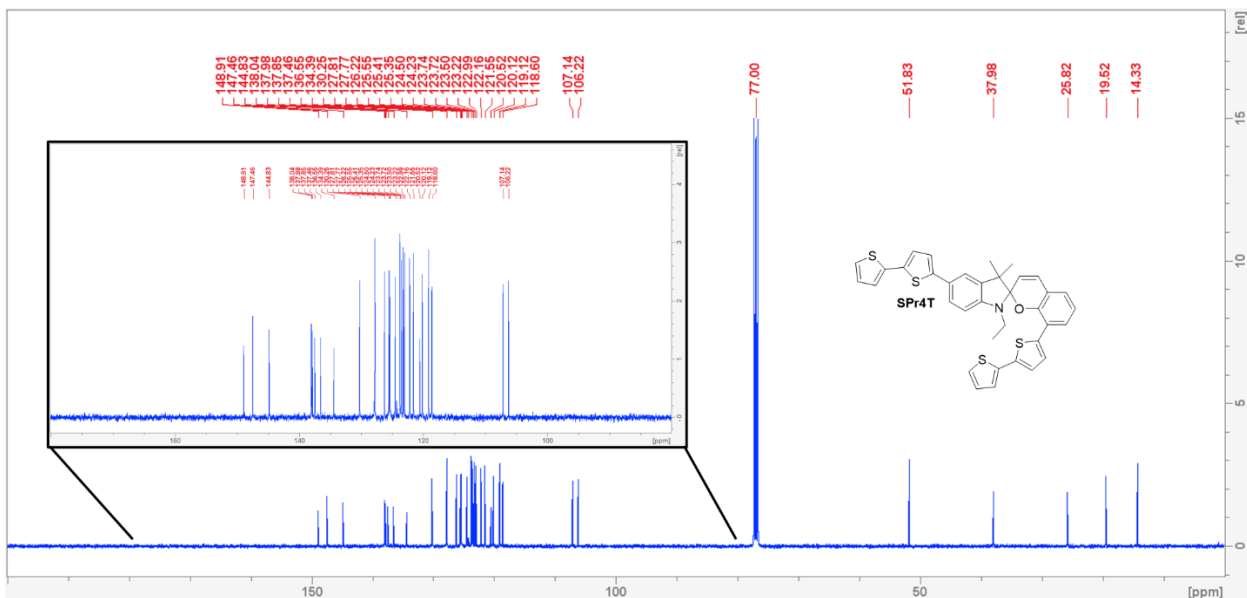


Figure S15. ^{13}C -NMR of SPr4T in CDCl_3 at 100 MHz and 25 °C.

5. Cyclic Voltammetry

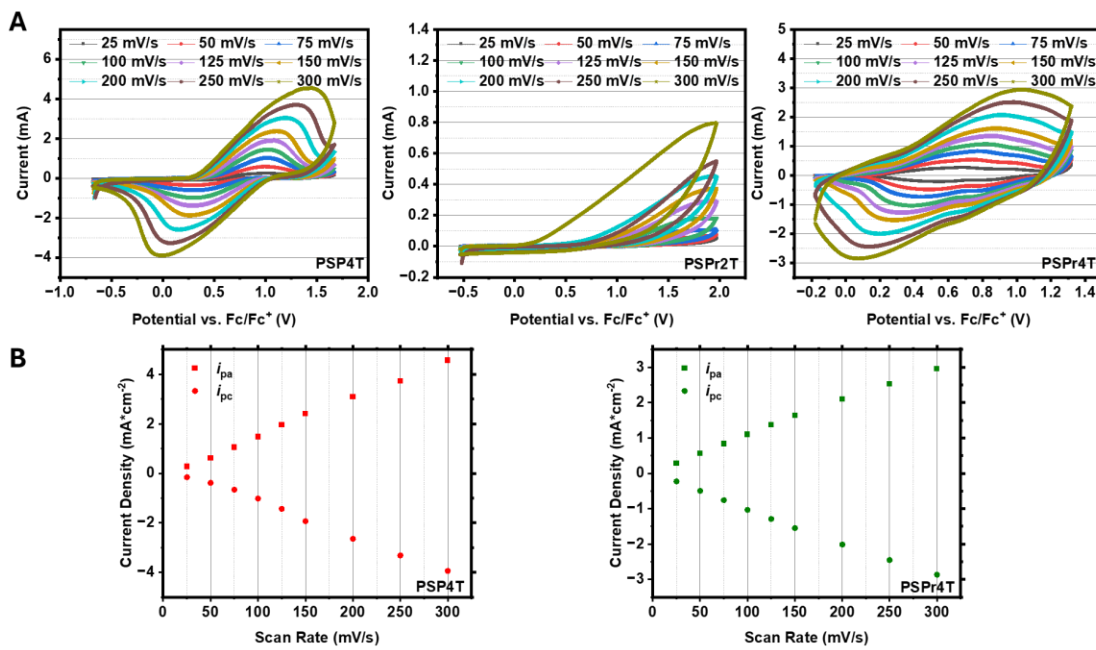


Figure S16. (A) Cyclic-voltammetry measurements with different scan rates (25, 50, 75, 100, 125, 150, 200, 250, and 300 mV/s) for PSP4T (left), PSPr2T (middle), and PSPr4T (right) in 0.1 M Bu_4NPF_6 /MeCN electrolyte. Referenced to the ferrocene redox couple. (B) i_{pc}/i_{pa} as a function of scan-rate for PSP4T (left) and PSPr4T (right).

Table S2. Anodic/Cathodic peak current (i_{pa}/i_{pc}) as a function of voltage scan-rate for PSP2T.

| Polymer | Scan Rate (mV·s ⁻¹) | i_{pa} (mA·cm ⁻²) | i_{pc} (mA·cm ⁻²) |
|---------|---------------------------------|---------------------------------|---------------------------------|
| PSP2T | 25 | -0.0179 | 0.02353 |
| PSP2T | 50 | -0.03114 | 0.03722 |
| PSP2T | 75 | -0.04325 | 0.05047 |
| PSP2T | 100 | -0.0557 | 0.06462 |
| PSP2T | 125 | -0.06883 | 0.07944 |
| PSP2T | 150 | -0.08151 | 0.09506 |
| PSP2T | 200 | -0.10528 | 0.12381 |
| PSP2T | 250 | -0.12757 | 0.15233 |
| PSP2T | 300 | -0.14829 | 0.18131 |

Table S3. Anodic/Cathodic peak current (i_{pa}/i_{pc}) as a function of voltage scan-rate for PSP4T.

| Polymer | Scan Rate (mV·s ⁻¹) | i_{pa} (mA·cm ⁻²) | i_{pc} (mA·cm ⁻²) |
|---------|---------------------------------|---------------------------------|---------------------------------|
| PSP4T | 25 | -0.15676 | 0.26967 |
| PSP4T | 50 | -0.3871 | 0.62139 |
| PSP4T | 75 | -0.66101 | 1.05093 |
| PSP4T | 100 | -1.02207 | 1.47736 |
| PSP4T | 125 | -1.43605 | 1.95048 |
| PSP4T | 150 | -1.93096 | 2.41426 |
| PSP4T | 200 | -2.64375 | 3.08347 |
| PSP4T | 250 | -3.31919 | 3.72779 |
| PSP4T | 300 | -3.94482 | 4.56819 |

Table S4. Anodic/Cathodic peak current (i_{pa}/i_{pc}) as a function of voltage scan-rate for PSPr4T.

| Scan Rate (mV·s ⁻¹) | i_{pa} (mA·cm ⁻²) | i_{pc} (mA·cm ⁻²) | Scan Rate (mV·s ⁻¹) |
|---------------------------------|---------------------------------|---------------------------------|---------------------------------|
| PSPr4T | 25 | -0.22977 | 0.28127 |
| PSPr4T | 50 | -0.49915 | 0.55857 |
| PSPr4T | 75 | -0.76061 | 0.83588 |
| PSPr4T | 100 | -1.03594 | 1.09932 |
| PSPr4T | 125 | -1.29145 | 1.37663 |
| PSPr4T | 150 | -1.55093 | 1.63611 |
| PSPr4T | 200 | -2.01443 | 2.09564 |
| PSPr4T | 250 | -2.45416 | 2.53141 |
| PSPr4T | 300 | -2.86814 | 2.95331 |

6. Electrochromic Characterization

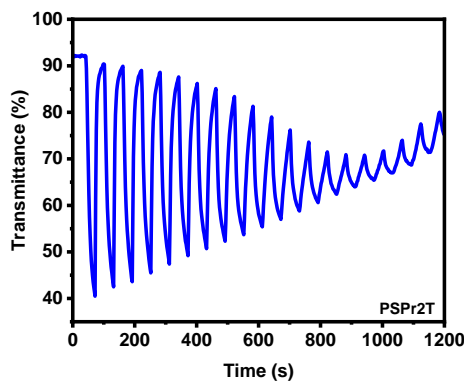


Figure S17. Electrochromic cycling stability measurements for PSPr2T on glass-ITO in 0.1M Bu₄NPF₆/PC electrolyte.

Table S5. Spectroelectrochemistry measurements for PSP2T, PSPr2T, PSP4T, and PSPr4T.

| Potential (V) | ΔAbs. at λ_{\max} | | | |
|---------------|---------------------------|--------------------|-------------------|--------------------|
| | PSP2T (410 nm) | PSPr2T (393 nm) | PSP4T (444 nm) | PSPr4T (438 nm) |
| -1.8 | 1.56581 | -- | -- | -- |
| -1.6 | 1.56579 | -- | -- | -- |
| -1.4 | 1.56414 | -- | 1.00784 | -- |
| -1.2 | 1.56526 | 0.99639 | 0.96978 | 0.61372 |
| -1.0 | 1.56599 | 0.99828 | 0.95852 | 0.61372 |
| -0.8 | 1.56654 | 0.99956 | 0.9458 | 0.61459 |
| -0.6 | 1.56702 | 0.99985 | 0.9388 | 0.61497 |
| -0.4 | 1.56782 | 1.00149 | 0.93359 | 0.61521 |
| -0.2 | 1.56687 | 1.00247 | 0.9279 | 0.61581 |
| 0 | 1.5652 | 1.01472 | 0.92096 | 0.61569 |
| + 0.2 | 1.56632 | 1.01535 | 0.90738 | 0.61641 |
| + 0.4 | 1.56516 | 1.01571 | 0.90263 | 0.6159 |
| + 0.6 | 1.56587 | 1.01574 | 0.89478 | 0.6108 |
| + 0.8 | 1.56502 | 1.01641 | 0.85671 | 0.60238 |
| + 1.0 | 1.56414 | 1.01587 | 0.84228 | 0.59928 |
| + 1.2 | 1.53796 | 1.00835 | 0.83104 | 0.59341 |
| + 1.4 | 1.40595 | 0.93688 | 0.78561 | 0.55248 |
| + 1.6 | 1.06562 | 0.77984 | 0.60235 | 0.45309 |
| + 1.8 | 0.9473 | 0.68316 | 0.45395 | 0.37248 |
| + 2.0 | -- | 0.66679 | 0.44544 | 0.34948 |

Table S6. Spectroelectrochemistry measurements for PSP2T, PSPr2T, PSP4T, and PSPr4T.

| Potential (V) | ΔAbs. at λ_{\max} | | | |
|---------------|---------------------------|--------------------|--------------------|-------------------|
| | PSP2T (954 nm) | PSPr2T (940 nm) | PSP4T (1100 nm) | PSPr4T (930nm) |
| -1.8 | 0.15942 | -- | -- | -- |
| -1.6 | 0.15958 | -- | -- | -- |
| -1.4 | 0.15972 | -- | -0.0209 | -- |
| -1.2 | 0.16001 | 0.0268 | -0.02528 | 0.08419 |
| -1.0 | 0.16018 | 0.02511 | -0.0263 | 0.08186 |
| -0.8 | 0.16056 | 0.02403 | -0.02635 | 0.08061 |
| -0.6 | 0.16101 | 0.02303 | -0.02702 | 0.0796 |
| -0.4 | 0.16233 | 0.02243 | -0.02725 | 0.07862 |
| -0.2 | 0.16373 | 0.02191 | -0.02734 | 0.07783 |
| 0 | 0.16443 | 0.02198 | -0.02734 | 0.0774 |
| + 0.2 | 0.16507 | 0.02128 | -0.02693 | 0.07794 |
| + 0.4 | 0.1664 | 0.02041 | -0.02475 | 0.08207 |
| + 0.6 | 0.16732 | 0.02102 | -0.01132 | 0.09002 |
| + 0.8 | 0.16781 | 0.02167 | 0.10984 | 0.09935 |
| + 1.0 | 0.17567 | 0.025 | 0.15437 | 0.1029 |
| + 1.2 | 0.30901 | 0.03891 | 0.18622 | 0.10618 |
| + 1.4 | 0.84814 | 0.10544 | 0.289 | 0.12655 |
| + 1.6 | 1.3821 | 0.42341 | 0.62853 | 0.25471 |
| + 1.8 | 1.61529 | 0.72419 | 0.79518 | 0.43793 |
| + 2.0 | -- | 0.77218 | 0.85062 | 0.51856 |

Table S7. Stability measurements for PSP2T, PSPr2T, PSP4T, and PSPr4T in 0.1 M Bu₄NPF₆/PC.

| PSP2T | PSPr2T | PSP4T | PSPr4T |
|---------|--------|----------|----------|
| 0.4584% | 45.63% | 4.17374% | 3.93463% |

Table S8. CIELAB Chromaticity Coordinates.

| Entry | L* | a* | b* |
|----------|------|------|-------|
| PSP2T | 69.7 | 3.8 | 21.8 |
| PSP2Tox | 57.8 | 6.8 | 10.2 |
| PSP4T | 73.9 | 16.2 | 56.6 |
| PSP4Tox | 59.3 | -2.7 | -10.4 |
| PSPr2T | 78.8 | -2 | 23.3 |
| PSPr2Tox | 76.5 | 4.9 | 15 |
| PSPr4T | 70.4 | 11.9 | 26.7 |
| PSPr4Tox | 71.2 | -2.1 | -2.4 |

7. Atomic Force Microscopy

Atomic force microscopy (AFM) was measured on a Digital Instrument Veeco AFM in standard tapping mode using a Si cantilever.⁴ Polymer films were prepared via electrochemical oxidative polymerization on glass-ITO substrates as previously described. The set point for all films is fixed within range of 0.70 to 1.5 nA magnitude with integral and proportional gains of 0.1 and 0.2 respectively. The scan speed is constant at 0.5 Hz in tapping mode. Nasoscope 6.13r1 and WSxM 5.0 software was used to acquire and analyze data respectively.

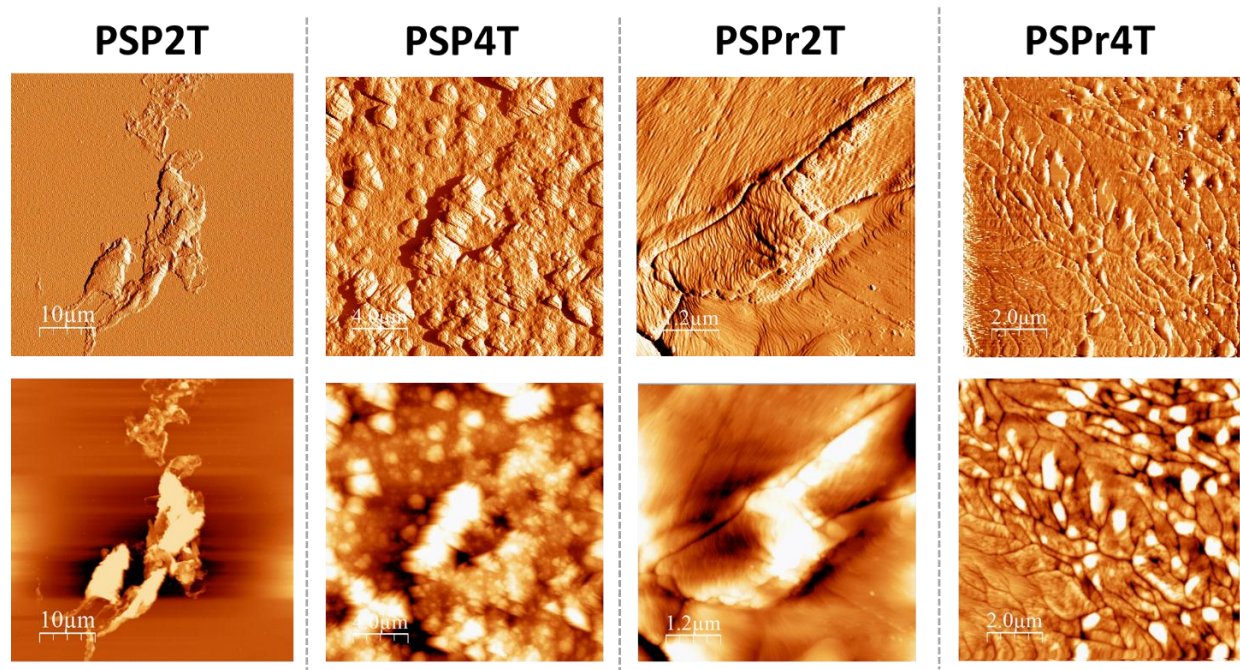


Figure S18. AFM phase (top) and height (bottom) images for PSP2T, PSP4T, PSPr2T, and PSPr4T with larger scan areas.

8. References

- (1) Reddington, M. V. Synthesis and Properties of Phosphonic Acid Containing Cyanine and Squaraine Dyes for Use as Fluorescent Labels. *Bioconjugate Chem.* **2007**, *18* (6), 2178–2190. <https://doi.org/10.1021/bc070090y>.
- (2) Sommer, M.; Komber, H. Spiropyran Main-Chain Conjugated Polymers. *Macromolecular Rapid Communications* **2013**, *34* (1), 57–62. <https://doi.org/10.1002/marc.201200688>.
- (3) Wagner, K.; Zanoni, M.; Elliott, A. B. S.; Wagner, P.; Byrne, R.; Florea, L. E.; Diamond, D.; Gordon, K. C.; Wallace, G. G.; Officer, D. L. A Merocyanine-Based Conductive Polymer. *J. Mater. Chem. C* **2013**, *1* (25), 3913–3916. <https://doi.org/10.1039/C3TC30479E>.
- (4) Saini, K.; Nair, A. N.; Yadav, A.; Enriquez, L. G.; Pollock, C. J.; House, S. D.; Yang, S.; Guo, X.; Sreenivasan, S. T. Nickel-Based Single-Molecule Catalysts with Synergistic Geometric Transition and Magnetic Field-Assisted Spin Selection Outperform RuO₂ for Oxygen Evolution. *Advanced Energy Materials* **2023**, *13* (42), 2302170. <https://doi.org/10.1002/aenm.202302170>.
- (5) Chai, J.-D.; Head-Gordon, M. Long-Range Corrected Hybrid Density Functionals with Damped Atom–Atom Dispersion Corrections. *Phys. Chem. Chem. Phys.* **2008**, *10* (44), 6615–6620. <https://doi.org/10.1039/B810189B>.
- (6) Franc, M. M.; Pietro, W. J.; Hehre, W. J.; Binkley, J. S.; Gordon, M. S.; DeFrees, D. J.; Pople, J. A. Self-consistent Molecular Orbital Methods. XXIII. A Polarization-type Basis Set for Second-row Elements. *The Journal of Chemical Physics* **1982**, *77* (7), 3654–3665. <https://doi.org/10.1063/1.444267>.
- (7) Hehre, W. J.; Ditchfield, R.; Pople, J. A. Self—Consistent Molecular Orbital Methods. XII. Further Extensions of Gaussian—Type Basis Sets for Use in Molecular Orbital Studies of Organic Molecules. *The Journal of Chemical Physics* **1972**, *56* (5), 2257–2261. <https://doi.org/10.1063/1.1677527>.
- (8) Frisch, M. J.; Trucks, G. W.; Schlegel, H. B.; Scuseria, G. E.; Robb, M. A.; Cheeseman, J. R.; Scalmani, G.; Barone, V.; Petersson, G. A.; Nakatsuji, H.; Li, X.; Caricato, M.; Marenich, A. V.; Bloino, J.; Janesko, B. G.; Gomperts, R.; Mennucci, B.; Hratchian, H. P.; Ortiz, J. V.; Izmaylov, A. F.; Sonnenberg, J. L.; Williams-Young, D.; Ding, F.; Lipparini, F.; Egidi, F.; Goings, J.; Peng, B.; Petrone, A.; Henderson, A.; Ranasinghe, D.; Zakrzewski, V. G.; Gao, J.; Rega, N.; Zheng, G.; Laing, W.; Hada, M.; Ehara, M.; Toyota, K.; Fukuda, R.; Hasegawa, J.;

- Ishida, M.; Nakajima, T.; Honda, Y.; Kitao, O.; Nakai, H.; Vreven, T.; Throssell, K.; Montomgery Jr., J. A.; Peralta, J. E.; Ogliaro, F.; Bearpark, M. J.; Heyd, J. J.; Brothers, E. N.; Kudin, K. N.; Staroverov, V. N.; Keith, T. A.; Kobayashi, R.; Normand, J.; Raghavachari, K.; Rendell, A. P.; Burant, J. C.; Lyengar, S. S.; Tomasi, J.; Cossi, M.; Millam, J. M.; Klene, M.; Adamo, C.; Cammi, R.; Ochterski, J. W.; Martin, R. L.; Morokuma, K.; Farkas, O.; Foresman, J. B.; Fox, D. J. Gaussian 16, Revision B.01.
- (9) Runge, E.; Gross, E. K. U. Density-Functional Theory for Time-Dependent Systems. *Phys. Rev. Lett.* **1984**, *52* (12), 997–1000. <https://doi.org/10.1103/PhysRevLett.52.997>.
- (10) Gross, E. K. U.; Kohn, W. Time-Dependent Density-Functional Theory. In *Advances in Quantum Chemistry*; Löwdin, P.-O., Ed.; Academic Press, 1990; Vol. 21, pp 255–291. [https://doi.org/10.1016/S0065-3276\(08\)60600-0](https://doi.org/10.1016/S0065-3276(08)60600-0).
- (11) Heinze, H. H.; Görling, A.; Rösch, N. An Efficient Method for Calculating Molecular Excitation Energies by Time-Dependent Density-Functional Theory. *The Journal of Chemical Physics* **2000**, *113* (6), 2088–2099. <https://doi.org/10.1063/1.482020>.
- (12) *Chemcraft - Graphical Software for Visualization of Quantum Chemistry Computations*. Version 1.8, Build 682. <https://www.chemcraftprog.com>.